DOI: 10.1002/ejic.201100422

The Effect of Trigonal Bipyramidal Distortion of Pentacoordinate $V^{IV}O^{2+}$ Species on their Structural, Electronic and Spectroscopic Parameters

Giovanni Micera[a] and Eugenio Garribba*[a]

Keywords: Vanadium / Structure elucidation / EPR spectroscopy / UV/Vis spectroscopy / Vibrational spectroscopy / Density functional calculations

The effect of trigonal bipyramidal distortion of pentacoordinate $V^{IV}O^{2+}$ species on their structural, electronic and spectroscopic parameters was calculated by DFT methods. In particular i) the bis chelated species with $[VO(LH_{-1})_2]^{2-}$ stoichiometry formed in water with five α-hydroxycarboxylic acid ligands [glycolic (glycH), lactic (lactH), 2-hydroxyisobutyric (2-hibH), 2-ethyl-2-hydroxybutyric (2-ehbH) and 2-isopropyl-2-hydroxybutyric (2-*i*PrhbH) acids], ii) the bis complexes $[VOL_2]$ formed in the solid state with three salicylaldimine derivatives [*N*-methylsalicylaldimine (MeSalH), *N*-isopropyl-*o*-methylsalicylaldimine (*i*Pr-MeSalH) and *N*-methyl-*o*-*tert*-butyl-*p*-methylsalicylaldimine (*t*Bu-MeSalH)] and iii) the solid bis chelated compounds with composition $[VOL_2]$ formed with aminophenolate ligands {2-[(dimethylamino)methyl]-phenol (NMe_2phenH), 2-(piperid-1-ylmethyl)-4-methylphenol (Pip-4MephenH), 2-[(dimethylamino)methyl]-6-*tert*-butylphenol (NMe_2-*t*BuphenH)} were examined. The variation of the structural [bond lengths, axial and equatorial angles, value of ΔE(solv), molecular orbital composition and electronic structure], EPR ($|A_x - A_y|$, $|A_{iso}|$, $|A_z|$ and $|g_x - g_y|$), UV/Vis ($\Delta\lambda = \lambda_2 - \lambda_3$ and λ_1), IR ($\nu_{V=O}$) and electron spin echo envelope modulation (ESEEM) spectroscopic parameters ($|A_{iso}^N|$, C_Q and η) as a function of the structural index of trigonality, $\tau = (\beta - \alpha)/60$ (where β and α are the angles subtended by vanadium between the two axial and equatorial donors), is illustrated.

Introduction

The biological importance of vanadium is well known.[1] Furthermore, vanadium compounds exhibit a wide variety of pharmacological properties including insulin-like effects.[2,3]

The most stable oxidation states of vanadium are +III, +IV and +V. Vanadium(IV) complexes are most commonly observed as compounds of the oxidovanadium ion, $V^{IV}O^{2+}$,[1,4] and this chemical form seems to be the most important in blood serum.[5] The main coordination geometries of $V^{IV}O^{2+}$ are square pyramidal and, less often, distorted octahedral. However, the pentacoordinate arrangement in the presence of bulky groups can undergo a trigonal bipyramidal distortion, which may influence the enzymatic and/or biological activity of V proteins. For example, a trigonal bipyramidal distortion has been proposed by Santoni and Rehder for the reduced form of bromoperoxidase from the marine brown alga *Ascophyllum nodosum*.[6] Therefore, to correctly study these systems in the absence of single-crystal X-ray diffraction analysis, it is fundamental to have a tool to characterize the geometry of a $V^{IV}O^{2+}$ species and its eventual distortion.

Computational approaches have been revealed to be useful in the prediction of structural details, electronic properties and spectroscopic features of many transition metal complexes and they have been recently reviewed.[7–10] In particular, it has been shown that ab initio and semiempirical quantum-chemical methods,[8] DFT simulations,[7] ligand field molecular mechanics,[10] and the combined use of ligand field theory (LFT) and DFT,[9] can be efficiently and reliably used to compute the structure of metal compounds. Of course, the most appropriate method depends mainly on the type of molecular proprieties to be predicted; for example, LFT still represents the most valid technique to calculate the electronic properties of many complexes including those formed by $V^{IV}O^{2+}$.[11]

DFT methods are acquiring a growing popularity;[7] they have the advantage that they can be performed with many program packages, available commercially or free of charge, and can be used on large molecules with high efficiency, in a user friendly manner and with a low computational cost. In particular, DFT simulations reproduce EPR, UV/Vis and IR spectra well and allow the connection of the spectral properties to the specific molecular orbital (MO) composition and electronic configuration. Therefore, it is plausible that such methods may relate the trigonal bipyramidal distortion of a $V^{IV}O^{2+}$ species to its spectroscopic parameters.

[a] Dipartimento di Chimica and Centro Interdisciplinare per lo Sviluppo della Ricerca Biotecnologica e per lo Studio della Biodiversità della Sardegna, Università di Sassari,
Via Vienna 2, 07100 Sassari, Italy
Fax: +39-079-229559
E-mail: garribba@uniss.it

Supporting information for this article is available on the WWW under http://dx.doi.org/10.1002/ejic.201100422.

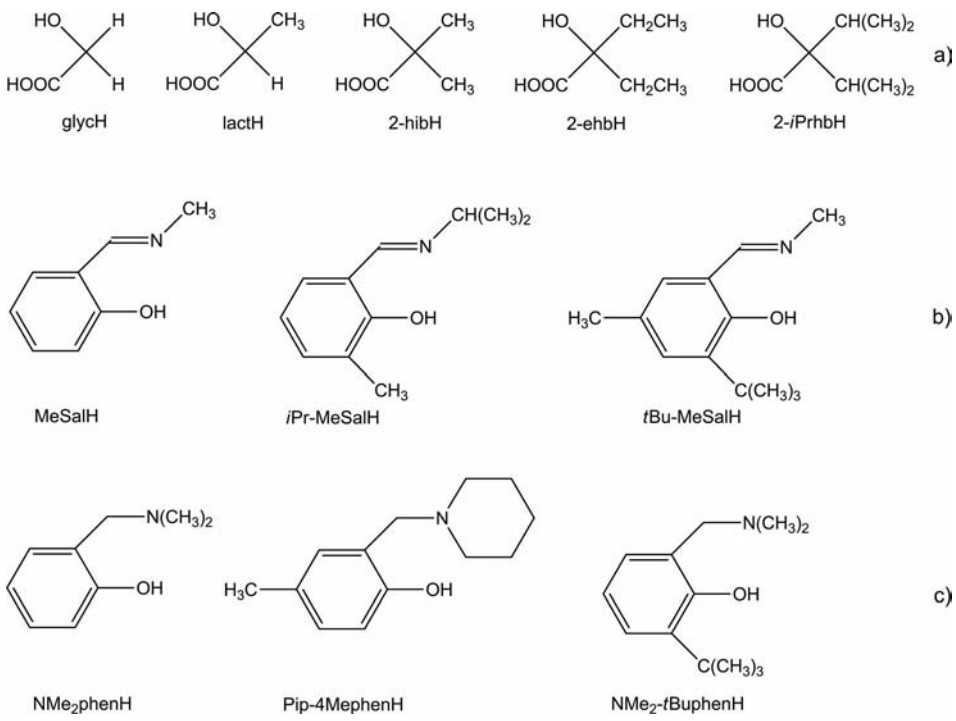

Scheme 1. The three classes of ligands studied: (a) α-hydroxycarboxylic acids, (b) salicylaldimine and (c) aminophenol derivatives.

The degree of distortion of a square pyramidal structure towards trigonal bipyramidal can be described by the structural index of trigonality, $\tau = (\beta - \alpha)/60$, where β is the angle subtended by vanadium between the two apical donors and α is the angle between the two equatorial donors ($\beta > \alpha$).[12]

To date, contrasting results have been published in the literature. On one hand, it has been reported that with the increase of steric hindrance of the substituents on the α-carbon atom of α-hydroxycarboxylate ligands, on the imine nitrogen and in *ortho* position to the phenolate of salicylaldiminate derivatives, the trigonal bipyramidal distortion increases; such a distortion results in a rhombic EPR spectrum[13,14] and a four-band electronic absorption spectrum.[14] Conversely, van Koten and coworkers suggested that for $V^{IV}O^{2+}$ complexes formed by aminophenolate ligands, the effect of the distortion cannot be detected spectroscopically.[15]

To clarify the debate, in this work we applied DFT methods to calculate how the structural [bond lengths, axial and equatorial angles, the value of ΔE(solv), the MO composition and electronic structure] and EPR, UV/Vis, IR and ESEEM spectroscopic parameters vary as a function of the degree of distortion towards trigonal bipyramidal, expressed by the value of τ. Three series of complexes were taken into account: those formed by α-hydroxycarboxylate ligands,[14,16] salicylaldimine derivatives[13] and aminophenolate ligands[15,17] (Scheme 1). In particular, i) the bis chelated species $[VO(LH_{-1})_2]^{2-}$ formed in water by five α-hydroxycarboxylic acid ligands [glycolic (glycH), lactic (lactH), 2-hydroxyisobutyric (2-hibH), 2-ethyl-2-hydroxybutyric (2-ehbH) and 2-isopropyl-2-hydroxybutyric (2-*i*PrhbH) acids],[18] ii) the bis complexes $[VOL_2]$ formed in the solid state by three salicylaldimine derivatives [*N*-methylsalicylaldimine (MeSalH), *N*-isopropyl-*o*-methylsalicylaldimine (*i*Pr-MeSalH) and *N*-methyl-*o*-*tert*-butyl-*p*-methylsalicylaldimine (*t*Bu-MeSalH)] and iii) the solid bis chelated compounds $[VOL_2]$ formed by aminophenolate ligands {2-[(dimethylamino)methyl]phenol (NMe_2phenH), 2-(piperid-1-ylmethyl)-4-methylphenol (Pip-4MephenH), 2-[(dimethylamino)methyl]-6-*tert*-butylphenol (NMe_2-*t*BuphenH)} were examined. The results may be useful to predict the effect of trigonal bipyramidal distortion on $V^{IV}O^{2+}$ species and help to understand, in the absence of X-ray diffractometric analysis, if a specific complex is distorted.

Results and Discussion

Variation of the Structural Parameters

α-Hydroxycarboxylate ligands form bis chelated complexes with $V^{IV}O^{2+}$ using the (COO^-, O^-) donor set.[14,16] It has been reported that the degree of distortion increases with the steric engagement of the substituents on the α-carbon atom: (H, H) for glyc, (H, Me) for lact, (Me, Me) for 2-hib, (Et, Et) for 2-ehb and (*i*Pr, *i*Pr) for 2-*i*Prhb.[14] The only X-ray structure reported in the literature for this kind of species is with benzilic acid (benzH), $Na(NEt_4)[VO(benzH_{-1})_2]$,[19] in which the equatorial distances V–O(alkoxido) are 1.90 and 1.93 Å and the axial distances V–O(carboxylato) are 1.97 Å; the equatorial and axial angles O–V–O are 132.9 and 151.6°, respectively, and the τ value is 0.312.

Salicylaldimine and aminophenol derivatives bind vanadium through the (N, O^-) couple, with the nitrogen atoms (imine or amine) and the phenolate oxygen atoms in *trans* position. The steric hindrance of the ligands changes progressively with changing the substituent R on the nitrogen atom and R′ on the carbon atom in *ortho* position to the coordinating phenolate group (Scheme 1), which results in a significant increase of the trigonal bipyramidal distortion. In particular, with salicylaldiminate ligands τ is 0.55 for $[VO(MeSal)_2]$ (Me, H), 0.58 for $[VO(i\text{Pr-MeSal})_2]$ (*i*Pr, Me) and 0.70 for $[VO(t\text{Bu-MeSal})_2]$ (Me, *t*Bu),[13] whereas with aminophenolate species τ is 0.50 for $[VO(\text{Pip-4Mephen})_2]$ (piperidine ring, H), 0.59 for $[VO(NMe_2\text{phen})_2]$ ($2CH_3$, H) and 0.80 for $[VO(NMe_2\text{-}t\text{Buphen})_2]$ ($2CH_3$, *t*Bu).[15,17] The latter compound is, to the best of our knowledge, the $V^{IV}O^{2+}$ complex with the largest degree of distortion towards the trigonal bipyramid reported in the literature; the axial and equatorial angles are 125.3 and 173.3°, very close to the expected values of 120 and 180° for a trigonal bipyramid.[15]

The geometries of the $V^{IV}O^{2+}$ species were optimized by performing DFT calculations with the Gaussian 03 program (revision C.02).[20] The simulations were carried out both in the gas phase and in the solvent where they were formed within the framework of the polarizable continuum model.[21] The popular B3LYP functional was used:[22,23] its suitability to predict structures and energetics of several metal compounds, including vanadium, is well documented.[24] We recently evidenced that the 6-311G basis set allows calculation of a good agreement with the experimental bond lengths and angles for 32 representative $V^{IV}O^{2+}$ complexes with a reasonable calculation time.[25] Furthermore, the level of theory applied is enough to obtain a good prediction of the EPR and UV/Vis spectra.[26,27] A list of the selected structural parameters is reported in Table 1 and Table 2. In Figure 1 a representative $V^{IV}O^{2+}$ species for each of the three series is displayed.

The data presented in Table 1 suggest that the degree of distortion towards trigonal bipyramidal of the $[VO(LH_{-1})_2]^{2-}$ species formed by simple α-hydroxycarboxylate

Table 1. Structural parameters obtained from DFT calculations of $[VO(LH_{-1})_2]^{2-}$ complexes formed by α-hydroxycarboxylate ligands in the gas phase and solution.

Complex	V=O	V–O(eq)[a]	V–O(ax)[b]	O–V–O(eq)[a]	O–V–O(ax)[b]	τ
$[VO(glycH_{-1})_2]^{2-}$ (gas)	1.626	1.932, 1.932	2.067, 2.067	131.61	155.57	0.399
$[VO(glycH_{-1})_2]^{2-}$ (water)	1.635	1.914, 1.914	2.035, 2.035	131.83	154.60	0.380
$[VO(lactH_{-1})_2]^{2-}$ (gas)	1.628	1.932, 1.932	2.062, 2.062	131.62	155.40	0.396
$[VO(lactH_{-1})_2]^{2-}$ (water)	1.637	1.912, 1.912	2.037, 2.037	130.35	155.25	0.415
$[VO(2\text{-}hibH_{-1})_2]^{2-}$ (gas)	1.629	1.931, 1.931	2.057, 2.057	131.56	155.13	0.393
$[VO(2\text{-}hibH_{-1})_2]^{2-}$ (water)	1.639	1.908, 1.909	2.033, 2.034	130.78	155.26	0.408
$[VO(2\text{-}ehbH_{-1})_2]^{2-}$ (gas)	1.629	1.928, 1.931	2.052, 2.055	131.68	154.86	0.386
$[VO(2\text{-}ehbH_{-1})_2]^{2-}$ (water)	1.641	1.908, 1.910	2.031, 2.036	129.72	156.84	0.452
$[VO(2\text{-}i\text{PrhbH}_{-1})_2]^{2-}$ (gas)	1.630	1.925, 1.931	2.047, 2.048	131.31	153.94	0.377
$[VO(2\text{-}i\text{PrhbH}_{-1})_2]^{2-}$ (water)	1.644	1.903, 1.904	2.033, 2.038	128.82	157.55	0.479
$[VO(benzH_{-1})_2]^{2-}$ [c]	1.584	1.900, 1.931	1.970, 1.971	132.93	151.62	0.312

[a] V–O(alkoxido) bond. [b] V–O(carboxylato) bond. [c] X-ray structure reported in ref.[19]

Table 2. Structural parameters obtained from DFT calculations of the $[VOL_2]$ complexes formed by salicylaldimine and aminophenol derivatives in the gas phase and solution.

Complex	V=O	V–O(eq)[a]	V–N(ax)[b]	O–V–O(eq)[a]	N–V–N(ax)[b]	τ
$[VO(MeSal)_2]$ (gas)	1.606	1.926, 1.926	2.119, 2.119	127.48	164.84	0.623
$[VO(MeSal)_2]$ (water)	1.620	1.917, 1.917	2.118, 2.118	128.32	164.60	0.605
Exp.[c]	1.590	1.893, 1.893	2.097, 2.097	129.6	162.8	0.553
$[VO(i\text{Pr-MeSal})_2]$ (gas)	1.609	1.924, 1.924	2.122, 2.122	124.85	167.11	0.704
$[VO(i\text{Pr-MeSal})_2]$ (water)	1.622	1.916, 1.916	2.123, 2.123	126.41	166.12	0.662
Exp.[c]	1.599	1.912, 1.915	2.096, 2.098	129.31	164.17	0.581
$[VO(t\text{Bu-MeSal})_2]$ (gas)	1.610	1.926, 1.926	2.117, 2.117	121.37	170.27	0.815
$[VO(t\text{Bu-MeSal})_2]$ (water)	1.623	1.917, 1.917	2.116, 2.116	122.37	169.33	0.783
Exp.[c]	1.601	1.901, 1.903	2.076, 2.089	123.99	165.77	0.696
$[VO(NMe_2\text{phen})_2]$ (gas)	1.615	1.910, 1.910	2.191, 2.191	128.12	165.27	0.619
$[VO(NMe_2\text{phen})_2]$ (Et_2O)	1.621	1.905, 1.906	2.190, 2.191	128.50	163.50	0.583
Exp.[d]	1.599	1.883, 1.897	2.147, 2.155	130.02	165.13	0.585
$[VO(\text{Pip-4Mephen})_2]$ (gas)	1.616	1.909, 1.909	2.201, 2.201	127.39	166.16	0.646
$[VO(\text{Pip-4Mephen})_2]$ (Et_2O)	1.625	1.905, 1.905	2.199, 2.200	128.08	164.22	0.602
Exp.[e]	1.590	1.883, 1.899	2.166, 2.165	131.20	161.17	0.500
$[VO(NMe_2\text{-}t\text{Buphen})_2]$ (gas)	1.620	1.908, 1.908	2.210, 2.210	123.21	177.42	0.903
$[VO(NMe_2\text{-}t\text{Buphen})_2]$ (Et_2O)	1.624	1.908, 1.909	2.208. 2.210	123.29	176.80	0.891
Exp.[e]	1.598	1.904. 1.912	2.150, 2.151	125.33	173.32	0.800

[a] V–O(phenolato) bond. [b] V–N(imine) or V–N(amine) bond. [c] X-ray structure reported in ref.[13] [d] X-ray structure reported in ref.[17] [e] X-ray structure reported in ref.[15]

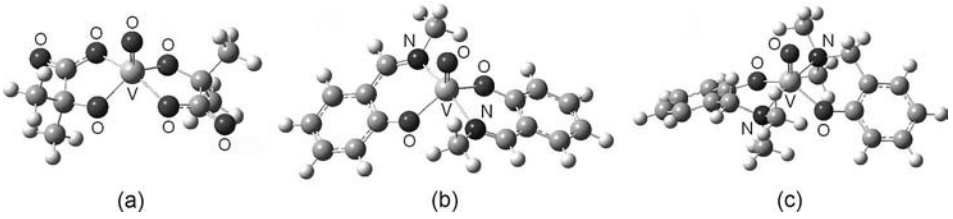

Figure 1. Optimized structures of the complexes $[VO(2\text{-}hibH_{-1})_2]^{2-}$ (a), $[VO(MeSal)_2]$ (b) and $[VO(NMe_2phen)_2]$ (c) calculated in solution by DFT methods at the B3LYP/6-311G level. $[VO(2\text{-}hibH_{-1})_2]^{2-}$ and $[VO(MeSal)_2]$ were simulated in water, $[VO(NMe_2phen)_2]$ in Et_2O.

ligands is $[VO(glycH_{-1})_2]^{2-} \approx [VO(lactH_{-1})_2]^{2-} \approx [VO(2\text{-}hibH_{-1})_2]^{2-} > [VO(2\text{-}ehbH_{-1})_2]^{2-} > [VO(2\text{-}i\text{PrhbH}_{-1})_2]^{2-}$ in the gas phase and $[VO(glycH_{-1})_2]^{2-} < [VO(lactH_{-1})_2]^{2-} \approx [VO(2\text{-}hibH_{-1})_2]^{2-} < [VO(2\text{-}ehbH_{-1})_2]^{2-} < [VO(2\text{-}i\text{Pr-}hbH_{-1})_2]^{2-}$ in aqueous solution. Surprisingly, the trend for the distortion in the gas phase and in water are opposite, suggesting that the solvation of the complex rather than the steric hindrance of the ligand determines the value of τ. To throw light on this problem, the total energy E of the two outer terms in the series – $[VO(glycH_{-1})_2]^{2-}$, the most distorted in the gas phase and the least in water, and $[VO(2\text{-}i\text{PrhbH}_{-1})_2]^{2-}$, the most distorted in water and the least in the gas phase – was calculated for τ that varies in the range 0.10–0.70 (Figure 2). It must be noted that the difference between the two curves corresponds to the ΔE(solv) of the complex. The minima of the curves in the gas phase and water fall to the τ value calculated through the optimization of the two structures {0.40 and 0.38 in the gas phase, and 0.38 and 0.48 in water for $[VO(glycH_{-1})_2]^{2-}$ and $[VO(2\text{-}i\text{PrhbH}_{-1})_2]^{2-}$, respectively}. As expected, ΔE(solv) is lower for the hydrophobic 2-*i*PrhbH ligand than for glycH. A comparison shows that the variation in the two cases is exactly opposite and, whereas for $[VO(glycH_{-1})_2]^{2-}$ the absolute value of ΔE(solv) slightly decreases with the trigonal bipyramidal distortion, for $[VO(2\text{-}i\text{PrhbH}_{-1})_2]^{2-}$ it increases significantly; consequently, in the second case the minimum in the curve representing E(solution) is reached for a higher value of τ.

However, on the whole, the results confirm the previous hypothesis that in aqueous solution the distortion towards trigonal bipyramidal of $[VO(LH_{-1})_2]^{2-}$ species increases from glycH to 2-*i*PrhbH.[14] DFT calculations also suggest that with increasing τ a slight difference between the two equatorial and two axial distances should be observed, confirming the features of the solid compound $Na(NEt_4)[VO(benzH_{-1})_2]$.[19] As an example, the optimized structure for $[VO(2\text{-}hibH_{-1})_2]^{2-}$ is shown in Figure 1 (a).

The results for $[VO(MeSal)_2]$, $[VO(i\text{Pr-}MeSal)_2]$ and $[VO(t\text{Bu-}MeSal)_2]$ on one hand and $[VO(NMe_2phen)_2]$, $[VO(Pip\text{-}4Mephen)_2]$ and $[VO(NMe_2\text{-}t\text{Buphen})_2]$ on the other indicate that the order of distortion in the gas phase and in the precipitating solvent (H_2O in the first case and Et_2O in the second) is identical: $[VO(MeSal)_2] < [VO(i\text{Pr-}MeSal)_2] < [VO(t\text{Bu-}MeSal)_2]$ for salicylaldimine derivatives and $[VO(NMe_2phen)_2] < [VO(Pip\text{-}4Mephen)_2] < [VO(NMe_2\text{-}t\text{Buphen})_2]$ for aminophenolate species. In these cases, the effect of the steric hindrance of the substituents

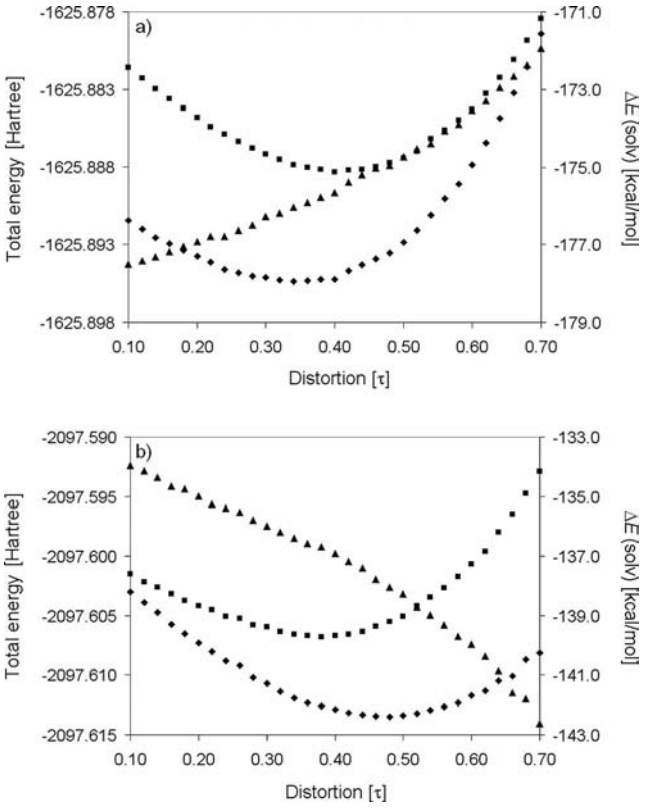

Figure 2. Variation of the total energy E in the gas phase (squares) and in aqueous solution (rhombi), and ΔE(solv) (triangles) for $[VO(glycH_{-1})_2]^{2-}$ (a) and $[VO(2\text{-}i\text{PrhbH}_{-1})_2]$ (b). The left and right hand axes refer to E and ΔE(solv) values, respectively.

on the nitrogen donor and aromatic ring is more important than the solvation of the complexes; in particular, the presence of a bulky group (e.g. *tert*-butyl) in the *ortho* position to the phenolic –OH causes an increase of the trigonal bipyramidal distortion larger than a bulky group on the imino or amino nitrogen atom (see Scheme 1). The structures of $[VO(MeSal)_2]$ and $[VO(NMe_2phen)_2]$ are presented in parts b and c of Figure 1. It can be seen that in the solid phase the experimental τ for $[VO(Pip\text{-}4Mephen)_2]$ is smaller than for $[VO(NMe_2phen)_2]$; however, if one only considers the steric hindrance of the substituents on the amino nitrogen atom, the opposite order is expected from DFT calculations. This suggests that solid state effects can be important in determining the experimental τ value.

The results indicate that N_{imine} or N_{amine} donors occupy the two axial positions, whereas O^-_{phen} donors are in the

two equatorial sites. The bond lengths and angles are in good agreement with those observed experimentally. All the distances are slightly overestimated confirming the general tendency of the all-electron calculations to overestimate the length of M–donor bonds, reported by Bühl and coworkers.[28]

Variation of the MO Composition and Electronic Structure

The electronic structure of one representative $V^{IV}O^{2+}$ species formed by each group of α-hydroxycarboxylate, salicylaldiminate and aminophenolate ligands is shown in Scheme S1 (Supporting Information). For clarity, the energy of the MOs is relative to highest occupied molecular orbital (HOMO) set as a reference to 0.0 eV.

Analysis of the electronic structure and MO composition has been performed choosing a coordinate system in which the V=O bond occupies the *z* axis, the two axial donors the *x* axis and the equatorial donors the *y* axis. Examination of Scheme S1 suggests that as a consequence of the trigonal bipyramidal distortion: i) the HOMO is always based on the V-d_{xy} orbital, ii) a significant splitting of the V-d_{xz} and V-d_{yz} orbitals, which should be degenerate for C_{4v} symmetry, is expected,[11] and iii) an inversion of the energy of V-$d_{x^2-y^2}$ and V-d_{z^2} orbitals can take place.

This is clarified in Scheme 2, where the variation of the energy of vanadium-based *d* orbitals for α-hydroxycarboxylate and salicylaldiminate complexes is depicted. By considering that in the first series τ varies from 0.38 to 0.48 and in the second from 0.62 to 0.82, one can imagine that the second part (Scheme 2, b) is roughly the continuation of the first (Scheme 2, a). It is noteworthy that with the value of τ, the splitting between V-d_{xz} and V-d_{yz} orbitals become larger; this happens because the distortion takes place mainly along the *y* axis, i.e. in the direction in which the angle between the *trans* donors approaches 120°. Moreover, the energy of the V-d_{z^2} orbital decreases and that of V-$d_{x^2-y^2}$ increases, resulting in an inversion of the two orbitals (part b of Scheme 2). For τ values around 0.6, as for the salicylaldiminate complexes, inversion between V-d_{z^2} and V-d_{yz} is also predicted (d–f in Scheme 2); however, this inversion can or cannot occur and other factors besides the trigonal bipyramidal distortion (e.g. the electronic properties of the ligands) can be important in realizing the real order of the energy levels (indeed, for aminophenolate complexes this inversion is not expected).

The most representative MOs of $[VO(2\text{-}i\text{PrhbH}_{-1})_2]^{2-}$ are shown in Figure S1 (see Supporting Information). The vanadium character of the V-d_{xy}, V-d_{xz} and V-d_{yz} based MOs is large (67–74%), because the possibility of π bonding with the equatorial ligands is reduced by the trigonal bipyramidal distortion. As noted elsewhere,[29] the V-d_{xz} and V-d_{yz} based MOs are engaged in a π bond with the O_{oxido}-p_x and O_{oxido}-p_y orbitals (Figure S1, c and e); their energy separation reflects the degree of distortion of the equatorial plane towards the trigonal bipyramid and increases from 0.70, to 0.74 and 0.81 eV for $[VO(glycH_{-1})_2]^{2-}$, $[VO(2\text{-}hibH_{-1})_2]^{2-}$ and $[VO(2\text{-}i\text{PrhbH}_{-1})_2]^{2-}$, respectively.

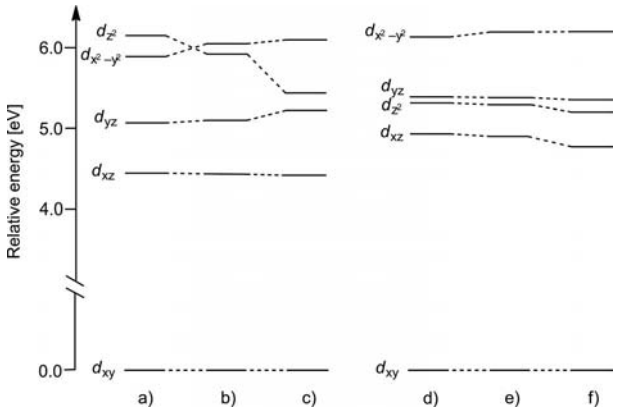

Scheme 2. Variation of the energy levels of vanadium based *d* orbitals (in water) of $[VO(glycH_{-1})_2]^{2-}$ (a), $[VO(2\text{-}hibH_{-1})_2]^{2-}$ (b), $[VO(2\text{-}i\text{PrhbH}_{-1})_2]^{2-}$ (c), $[VO(MeSal)_2]$ (d), $[VO(i\text{Pr-MeSal})_2]$ (e) and $[VO(t\text{Bu-MeSal})_2]$ (f).

The interaction of the V-$d_{x^2-y^2}$ orbital with the equatorial donors (mainly COO^- of the α-hydroxycarboxylate ligands) become strongest with increasing τ because the axial O–V–O angle rises from 154.6 to 157.6° from glycH to 2-*i*PrhbH and the COO^- groups approach the equatorial plane; this increases the energy of the V-$d_{x^2-y^2}$ orbital. On the contrary, interaction of the V-d_{z^2} orbital with the oxido-O donor weakens with increasing τ (10 vs. 2% from glycH to 2-*i*PrhbH) and, as a consequence, the energy of the V-d_{z^2} decreases and an inversion with V-$d_{x^2-y^2}$ is predicted. This is easily observed for $[VO(2\text{-}i\text{PrhbH}_{-1})_2]^{2-}$, for which V-$d_{z^2}$ is LUMO+3 (Figure S1, f), whereas V-$d_{x^2-y^2}$ is LUMO+8 (Figure S1, h).

Variation of the EPR Parameters (*g* and ^{51}V *A* Tensor)

Many reviews, books and articles have been published on the possibility of predicting the hyperfine coupling constants measured in the EPR spectra of transition metal complexes[7,30] and, specifically, of $V^{IV}O^{2+}$ complexes.[26,31]

According to the rule, the hyperfine coupling tensor ***A*** consists of two parts, the Fermi contact and the dipolar interaction (see DFT calculations section). The role of spin–orbit coupling is small for $V^{IV}O^{2+}$ compounds and, in a first approximation, can be considered as negligible.[31c] A DFT method for calculating the ***A*** tensor has been incorporated into Gaussian 03,[20] which, unlike other programs, does not include relativistic effects or spin–orbit coupling. A critical point in the prediction of A_z (by far the most important EPR parameter used in the characterization of $V^{IV}O^{2+}$ species) seems to be connected with the calculation of A_{iso}. It has been shown that for $V^{IV}O^{2+}$ complexes a good agreement with experimental A_{iso} values can be obtained with the nonrelativistic method and the use of half-and-half hybrid functionals.[31b] The recent demonstration that DFT calculations at the BHandHLYP/6-311G(d,p) level of theory are able to calculate A_z for $V^{IV}O^{2+}$ complexes with a mean deviation below 3% from the experi-

Table 3. *g* factors and ^{51}V hyperfine coupling constants obtained from DFT calculations of the $V^{IV}O^{2+}$ complexes formed by α-hydroxycarboxylate, salicylaldiminate and aminophenolate ligands.[a]

Complex	$g_{iso}^{calcd.}$	$g_{iso}^{exp.}$	$g_x^{calcd.}$	$g_y^{calcd.}$	$g_z^{calcd.}$	$g_x^{exp.}$	$g_y^{exp.}$	$g_z^{exp.}$	$\lvert A_{iso}\rvert^{calcd.}$	$\lvert A_{iso}\rvert^{exp.}$	$\lvert A_x\rvert^{calcd.}$	$\lvert A_y\rvert^{calcd.}$	$\lvert A_z\rvert^{calcd.}$	$\lvert A_x\rvert^{exp.}$	$\lvert A_y\rvert^{exp.}$	$\lvert A_z\rvert^{exp.}$	%$\lvert A_z\rvert$ [b]
$[VO(glycH_{-1})_2]^{2-}$	1.9763	1.971	1.9869	1.9782	1.9639	1.986	1.974	1.952	80.5	84.0	51.0	41.0	149.9	53.0	47.0	157.2	–4.6
$[VO(lactH_{-1})_2]^{2-}$	1.9764	1.970	1.9870	1.9781	1.9641	1.986	1.974	1.951	78.5	83.0	49.1	38.7	147.8	53.8	46.4	156.6	–5.5
$[VO(2\text{-}hibH_{-1})_2]^{2-}$	1.9765	1.970	1.9870	1.9781	1.9645	1.985	1.975	1.951	78.0	81.0	48.8	38.0	147.3	51.2	42.8	153.6	–3.8
$[VO(2\text{-}ehbH_{-1})_2]^{2-}$	1.9762	1.970	1.9871	1.9779	1.9635	1.985	1.975	1.950	77.6	80.0	49.9	36.4	146.4	51.6	42.4	154.6	–5.3
$[VO(2\text{-}i\text{Prhbh}_{-1})_2]^{2-}$	1.9760	[c]	1.9873	1.9777	1.9631	[c]	[c]	[c]	76.0	[c]	48.9	34.5	144.5	[c]	[c]	[c]	_
$[VO(MeSal)_2]$	1.9773	1.972	1.9869	1.9819	1.9631	1.983	1.981	1.951	89.3	91.4	51.0	59.3	157.4	53.1	60.0	161.0	–2.2
$[VO(i\text{Pr-MeSal})_2]$	1.9769	1.971	1.9871	1.9815	1.9621	1.983	1.981	1.949	88.5	90.7	49.8	59.2	156.4	51.8	59.4	161.0	–2.9
$[VO(t\text{Bu-MeSal})_2]$	1.9758	1.970	1.9876	1.9808	1.9590	1.984	1.979	1.947	86.0	88.2	46.3	58.4	153.4	47.8	59.4	157.3	–2.5
$[VO(NMe_2phen)_2]$	1.9756	1.972	1.9855	1.9791	1.9623	1.985	1.977	1.948	87.3	92.7	54.2	51.2	156.4	55.7	55.7	164.2	–4.8
$[VO(Pip\text{-}4Mephen)_2]$	1.9754	1.971	1.9854	1.9789	1.9621	1.985	1.977	1.947	86.8	92.7	53.6	50.7	155.9	55.6	55.4	164.5	–5.2
$[VO(NMe_2\text{-}t\text{Buphen})_2]$	1.9737	1.970	1.9856	1.9771	1.9585	1.983	1.976	1.945	84.0	89.7	51.9	47.4	152.7	54.9	55.9	162.5	–6.0

[a] Values of the ^{51}V hyperfine coupling constants given in 10^{-4} cm^{-1}. [b] Percent deviation from the experimental value calculated as $100 \times (|A_z|^{calcd.} - |A_z|^{exp.})/|A_z|^{exp.}$. [c] Value not reported in the literature.

mental values is encouraging.[26] The results of the simulations performed on the $V^{IV}O^{2+}$ complexes studied in this work are presented in Table 3.

If the components of the ***A*** tensor are expressed as absolute values, a general tendency to underestimate A_{iso} and A_z can be observed; the deviation of $|A_z|^{calcd.}$ for α-hydroxycarboxylate and aminophenolate complexes is approximately 5%, whereas that of salicylaldimine derivatives is lower than 3%. This confirms, as previously observed, that the agreement between $|A_z|^{calcd.}$ and $|A_z|^{exp.}$ is better for neutral complexes.[26]

The ***g*** tensor was calculated with the ORCA software,[32] which can use uncontracted multireference configuration interaction wavefunctions.[33] As a spin–orbit coupling operator, the spin–orbit mean field approximation was used as incorporated in the ORCA software. The values for g_{iso}, g_x, g_y and g_z are listed in Table 3. They are slightly overestimated with deviations from the experimental values of around 0.3, 0.1, 0.1 and 0.7%, respectively.

In agreement with the experimental data, the simulations predict that the symmetry reduction with respect to C_{4v} due to geometry distortion, results in a rhombic spectrum with three A ($A_z > A_x \neq A_y$) and three g ($g_z > g_x \neq g_y$) values; it has been proposed that the *x*,*y* anisotropy of the EPR spectra can be related to the *x*,*y* anisotropy in the geometric structure.[13,14]

On the basis of the DFT calculations, several parameters measured from an EPR spectrum, can be related to the trigonal bipyramidal distortion of a $V^{IV}O^{2+}$ species: i) $|A_x - A_y|$, which increases with increasing τ value (Figure 3), ii) $|A_{iso}|$, which decreases with increasing τ (Figure 4), iii) $|A_z|$, which decreases with increasing τ (Figure 5) and iv) $|g_x - g_y|$, which increases with increasing τ (Figure 6).

The correlation between $|A_x - A_y|$ and the value of τ has already been proposed for α-hydroxycarboxylate complexes,[14] whereas that between $|A_{iso}|$ and $|A_z|$ and τ is presented here for the first time. Therefore, if the coordination number, donor set and electric charge are fixed, a slight decrease of $|A_{iso}|$ and $|A_z|$ can be expected with the trigonal bipyramid distortion. It must be highlighted that, to obtain the correlation proposed, an accurate measurement of A_x and A_y is needed. This is not an easy task, because the EPR signals associated with the *x*,*y* regions are superimposed on the central part of the spectrum with each other and the *z* component; these difficulties increase when the values of A_x and A_y are close and their resonances are strongly over-

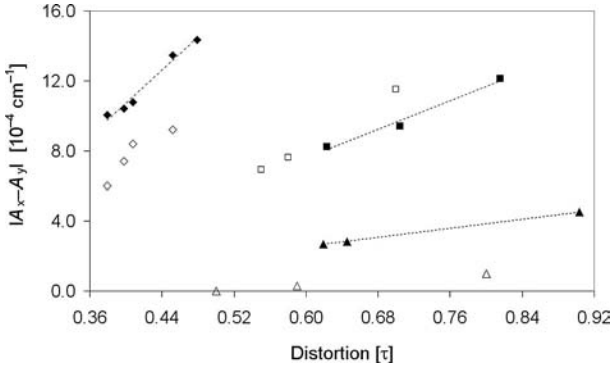

Figure 3. Variation of the $|A_x - A_y|$ parameter as a function of τ for $V^{IV}O^{2+}$ complexes formed by α-hydroxycarboxylate (rhombi), salicylaldiminate (squares) and aminophenolate ligands (triangles). The calculated and experimental values are shown as filled and empty symbols, respectively.

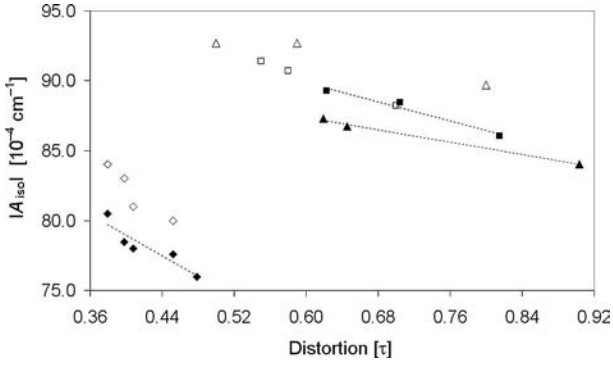

Figure 4. Variation of the $|A_{iso}|$ value as a function of τ for $V^{IV}O^{2+}$ complexes formed by α-hydroxycarboxylate (rhombi), salicylaldiminate (squares) and aminophenolate ligands (triangles). The calculated and experimental values are shown as filled and empty symbols, respectively.

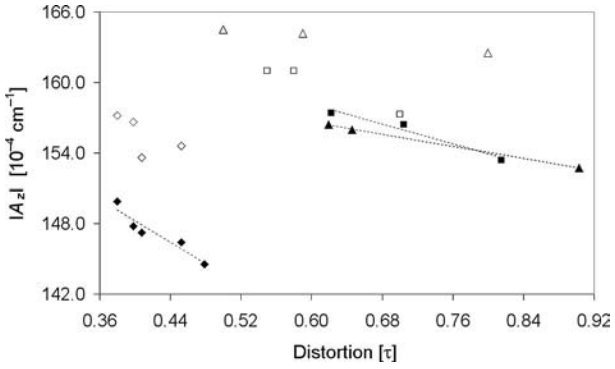

Figure 5. Variation of the $|A_z|$ value as a function of τ for $V^{IV}O^{2+}$ complexes formed by α-hydroxycarboxylate (rhombi), salicylaldiminate (squares) and aminophenolate ligands (triangles). The calculated and experimental values are shown as filled and empty symbols, respectively.

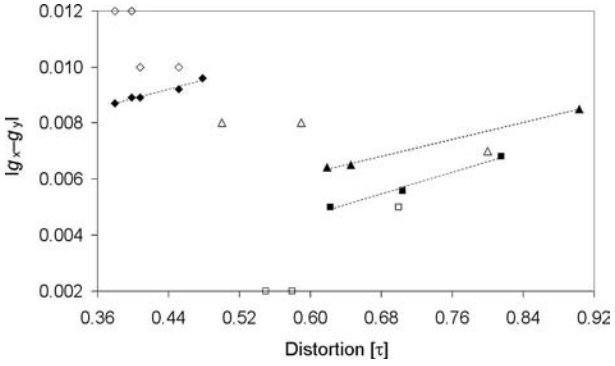

Figure 6. Variation of the $|g_x - g_y|$ parameter as a function of τ for $V^{IV}O^{2+}$ complexes formed by α-hydroxycarboxylate (rhombi), salicylaldiminate (squares) and aminophenolate ligands (triangles). The calculated and experimental values are shown as filled and empty symbols, respectively.

lapped. This is why correlation between $|A_x - A_y|$ and τ can be experimentally observed for salicylaldiminate[13] and α-hydroxycarboxylate complexes[14] and is not detected for aminophenolate species.[15]

DFT calculations also predict an increase of the $|g_x - g_y|$ parameter with the trigonal bipyramidal distortion (Figure 6). However, such an increase should be appreciable only if four decimal figures are reported; the fact that g values are usually measured with only three decimal figures and are characterized by a high degree of uncertainty due to the linewidth of the resonances imposes serious restrictions to the application of this correlation, and we believe that it will be very difficult to demonstrate experimentally. In addition, a slight decrease of g_{iso} and g_z as a function of τ is expected from examination of the data in Table 3.

Finally, it is interesting to plot the absolute values of the components of the dipolar tensor $\boldsymbol{T}$ as a function of τ (Figure S2, Supporting Information): $|T_y|$ increases with τ, $|T_x|$ and $|T_z|$ decrease and, consequently, in agreement with that predicted, $|A_z|$ decreases and the anisotropy parameter $|A_x - A_y|$ increases.

Variation of the Electronic Absorptions (λ_{max})

After recent implementations, time dependent DFT (TD-DFT) methods are now frequently used to calculate electronic transitions of metal complexes.[7,34,35] Such methods describe a given transition in terms of a linear combination of vertical excitations from occupied to virtual MOs and, consequently, only the dominant character of each transition and its contribution can be specified. TD-DFT also provides the electric dipole oscillator strength (f) of the transition from the ground to the excited state, which is related to the transition moment, thereby allowing the description of the electronic spectrum of a chemical compound in the UV/Vis region.

The experimental and calculated values of λ_{max} for d–d transitions are listed in Table 4, and the most important orbital transitions and their character, the excitation wavelengths and the oscillator strengths, calculated with functional B3LYP for $[VO(glycH_{-1})]^{2-}$, $[VO(MeSal)_2]$ and $[VO(NMe_2phen)_2]$ are given in Table 5. The main difference between the three classes of $V^{IV}O^{2+}$ compounds is that for α-hydroxycarboxylate and aminophenolate complexes four absorption bands in the region 400–900 nm are expected and for salicylaldiminate complexes five bands.

According to the results of the TD-DFT simulations, the four transitions of α-hydroxycarboxylate species are ligand field (LF) d–d transitions. In particular, they can be described as $d_{xy} \rightarrow d_{xz}$, $d_{xy} \rightarrow d_{yz}$, $d_{xy} \rightarrow d_{x^2-y^2}$ and $d_{xy} \rightarrow d_{z^2}$ excitations; the first two absorptions are almost pure d–d

Table 4. Electronic transitions in the visible region of the $V^{IV}O^{2+}$ complexes formed by α-hydroxycarboxylate, salicylaldiminate and aminophenolate ligands.[a]

Complex	$\lambda_4^{calcd.}$	$\lambda_3^{calcd.}$	$\lambda_2^{calcd.}$	$\lambda_1^{calcd.}$	$\lambda_4^{exp.}$	$\lambda_3^{exp.}$	$\lambda_2^{exp.}$	$\lambda_1^{exp.}$
$[VO(glycH_{-1})_2]^{2-}$	412.4	509.5	548.4	801.8	404	532	606	804
$[VO(lactH_{-1})_2]^{2-}$	415.0	510.8	548.8	812.9	409	536	602	820
$[VO(2\text{-}hibH_{-1})_2]^{2-}$	417.1	515.3	549.4	806.9	416	537	596	850
$[VO(2\text{-}ehbH_{-1})_2]^{2-}$	416.5	520.3	544.0	804.2	416	539	592	860
$[VO(2\text{-}i\text{PrhbH}_{-1})_2]^{2-}$	417.9	527.0	540.7	814.1	[b]	[b]	[b]	[b]
$[VO(MeSal)_2]$	449.2	513.3	539.6	753.4	–	532	592	833
$[VO(i\text{Pr-MeSal})_2]$	446.0	507.3	552.0	768.1	–	536	598	835
$[VO(t\text{Bu-MeSal})_2]$	451.8	509.8	597.3	799.0	–	519	623	850
$[VO(NMe_2phen)_2]$	401.0	543.3	581.4	854.7	397	541	≈ 600	877
$[VO(Pip\text{-}4Mephen)_2]$	402.3	547.6	583.6	862.3	404	541	625	880
$[VO(NMe_2\text{-}t\text{Buphen})_2]$	393.4	550.0	585.5	941.9	–	554	≈ 600	919

[a] Values given in nm. [b] Value not reported in the literature.

Table 5. Main calculated and experimental electronic transitions of $[VO(glycH_{-2})_2]^{2-}$ $[VO(MeSal)_2]$ and $[VO(NMe_2phen)_2]$.

Complex	Transition	Most important orbital excitation	Character/%	$\lambda^{calcd.[a]}$	$10^5 \times f^{calcd.}$	$\lambda^{exp.}/\varepsilon^{exp.[a,b]}$
$[VO(glycH_{-2})_2]^{2-}$	1	HOMO → LUMO	$d_{xy} \rightarrow d_{xz}$ (89.1)	801.8	32.2	804/22
	2	HOMO → LUMO+1	$d_{xy} \rightarrow d_{yz}$ (80.4)	548.4	58.9	606/27
	3	HOMO → LUMO+7	$d_{xy} \rightarrow d_{x^2-y^2}$ (69.0)	509.5	1.1	532/28
	4	HOMO → LUMO+8	$d_{xy} \rightarrow d_{z^2}$ (52.0)	412.4	54.3	404/35
$[VO(MeSal)_2]$	1	HOMO → LUMO+2	$d_{xy} \rightarrow d_{xz}$ (48.7)	753.4	0.8	833/14
	1	HOMO → LUMO	$d_{xy} \rightarrow \pi^*$(imine) (44.4)			
	2	HOMO → LUMO+3	$d_{xy} \rightarrow d_{z^2}$ (44.5)	539.6	1.0	592/45
	2	HOMO → LUMO+7	$d_{xy} \rightarrow d_{x^2-y^2}$ (34.9)			
	3	HOMO → LUMO+4	$d_{xy} \rightarrow d_{yz}$ (76.3)	513.3	122.8	532/62
	4	HOMO-1 → LUMO	π(arom + O^-_{phen}) → π^*(imine) (74.6)	447.3	4.3	
	5	HOMO-1 → LUMO+1	π(arom + O^-_{phen}) → π^*(imine) (54.7)	435.2	2.3	
	6	HOMO → LUMO+1	$d_{xy} \rightarrow \pi^*$(imine) (69.8)	385.9	132.6	
	7	HOMO → LUMO	$d_{xy} \rightarrow \pi^*$(imine) (47.8)	379.2	771.3	
	7	HOMO → LUMO+2	$d_{xy} \rightarrow d_{xz}$ (33.5)			
	8	HOMO-1 → LUMO	π(arom + O^-_{phen}) → π^*(imine) (89.6)	374.8	292.0	
$[VO(NMe_2phen)_2]$	1	HOMO → LUMO	$d_{xy} \rightarrow d_{xz}$ (65.4)	854.7	65.1	877
	1	HOMO-2 → LUMO	π(arom + O^-_{phen}) → d_{xz} (30.3)			
	2	HOMO → LUMO+1	$d_{xy} \rightarrow d_{yz}$ (60.3)	581.4	136.9	600
	3	HOMO → LUMO+5	$d_{xy} \rightarrow d_{x^2-y^2}$ (40.0)	543.3	2.1	541
	3	HOMO → LUMO+2	$d_{xy} \rightarrow d_{z^2}$ (21.0)			
	4	HOMO → LUMO+2	$d_{xy} \rightarrow d_{z^2}$ (32.9)	401.0	0.2	397
	4	HOMO → LUMO+5	$d_{xy} \rightarrow d_{x^2-y^2}$ (21.9)			
	5	HOMO-1 → LUMO	π(arom + O^-_{phen}) → d_{xz} (96.5)	365.0	2.9	
	6	HOMO-2 → LUMO	π(arom + O^-_{phen}) → d_{xz} (65.6)	344.6	33.5	
	6	HOMO → LUMO	$d_{xy} \rightarrow d_{xz}$ (31.4)			

[a] Value of λ given in nm. [b] Value of ε given in $M^{-1}cm^{-1}$.

bands, whereas the last two are slightly mixed with other excitations. The small value of *f* is consistent with their LF origin. The next electronic band is expected in the UV region below 300 nm.

For aminophenolate complexes, four *d*–*d* absorptions are calculated, in agreement with the experimental observations. However, with respect to α-hydroxycarboxylate complexes, the *d*–*d* character of the excitations diminishes and the bands are the result of a large mixing of excited configurations due to the low symmetry of the complexes; for example, the $d_{xy} \rightarrow d_{xz}$ (HOMO → LUMO) excitation for 65.4 and π(arom + O^-_{phen}) → d_{xz} (HOMO-2 → LUMO) for 30.3% contribute to the first state of $[VO(NMe_2phen)_2]$. Moreover, the $d_{xy} \rightarrow d_{x^2-y^2}$ and $d_{xy} \rightarrow d_{z^2}$ excitations that give rise to the third and fourth transition are strongly mixed, and the first ligand-to-metal charge transfer (LMCT) transition appears at wavelengths lower than 370 nm.

Finally, for $V^{IV}O^{2+}$ complexes formed by salicylaldiminates five bands are predicted in the visible region, but only three can be assigned to LF transitions (and, except that $d_{xy} \rightarrow d_{yz}$, they are mixed with MLCT transitions) with the other two being intraligand (LL) excitations. Furthermore, the second and third transitions on one hand and the fourth and fifth on the other should be very close in energy, with the consequence that they could collapse into two distinct absorptions and their resolution could be precluded. Below 400 nm, MLCT and LL bands with higher values of *f* are expected. Therefore, for this class of species the electronic absorption spectrum in the visible region is due to the mixing of several excitations and its interpretation is complicated.

From this picture, it emerges that $V^{IV}O^{2+}$ complexes of α-hydroxycarboxylate complexes constitute a special case in which only *d*–*d* absorptions are present in the UV/Vis spectrum from 900 to 300 nm and they can be easily detected and assigned. For aminophenolate and salicylaldiminate species, the interpretation of the electronic spectrum in the visible region is less simple as the *d*–*d* bands are strongly mixed with MLCT, LMCT and LL excitations, and finding a correlation between the experimental λ_{max} values and the structural parameters can be problematic. The lack of correlation observed by van Koten and coworkers for aminophenolate compounds may be traced to these observations.[15]

A correlation between the UV/Vis spectra of the α-hydroxycarboxylate complexes, the splitting of the two central bands ($\Delta\lambda = \lambda_2 - \lambda_3$) and the trigonal bipyramidal distortion has been discussed.[14] In particular, it was observed that $\Delta\lambda$ decreases with increasing τ. This can be confirmed by examination of Figure 7 where the calculated (filled rhombi) and experimental (empty rhombi) values of $\Delta\lambda$ are plotted as a function of τ. An analogous trend is found for $V^{IV}O^{2+}$ species formed with aminophenolate ligands (Figure 7, filled and empty triangles). Instead, as noted above, no correlation was found for salicylaldiminate complexes because of the absence of one of the four *d*–*d* bands and the mixing with MLCT and LL excitations.

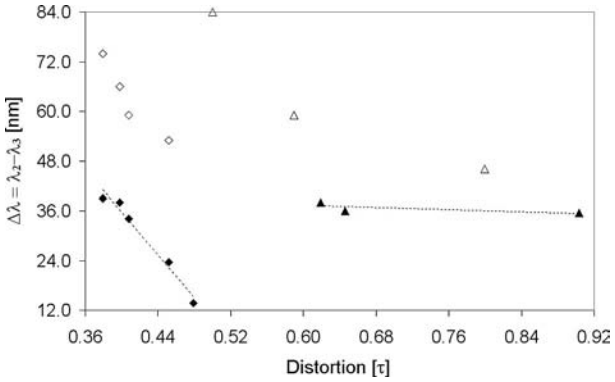

Figure 7. Variation of the $\Delta\lambda = \lambda_2 - \lambda_3$ parameter as a function of τ for $V^{IV}O^{2+}$ complexes formed by α-hydroxycarboxylate (rhombi) and aminophenolate ligands (triangles). The calculated and experimental values are shown as filled and empty symbols, respectively.

In all of the three series of compounds examined, a gradual increase of the value of λ_1 with τ can be observed. This band is mainly a LF transition and can be always described in terms of $d_{xy} \rightarrow d_{xz}$ excitation with respect to the other electronic absorptions; therefore, its shift is little disturbed by mixing with other excitations and/or the presence of other absorption bands. The calculated value of λ_1 as a function of τ is presented in Figure 8. An almost linear increase of λ_1 can be observed, which reproduces the experimental data well.

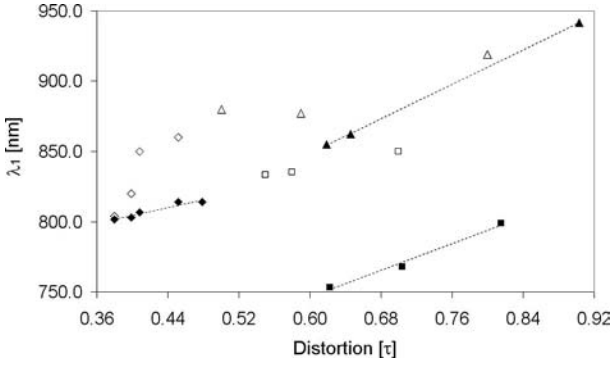

Figure 8. Variation of the λ_1 value as a function of τ for $V^{IV}O^{2+}$ complexes formed by α-hydroxycarboxylate (rhombi), salicylaldiminate (squares) and aminophenolate ligands (triangles). The calculated and experimental values are shown as filled and empty symbols, respectively.

Variation of V=O Stretching Frequency ($\nu_{V=O}$)

The prediction of harmonic vibrational frequencies on the basis of DFT methods has been pursued extensively.[36] Often, the frequencies predicted by GGA functionals such as BP86 and PBE agree well with those observed with errors usually below 10%.[7] It has been shown that such good agreement arises from a cancellation of errors, the underestimation of harmonic frequencies on one hand and the neglect of anharmonic frequencies on the other.[37] However, this systematic error is considered to be a fortunate coincidence of great help in the assignment of experimental spectra.[7] Recently, we shown that for $V^{IV}O^{2+}$ complexes formed by picolinate and quinolinate derivatives, the prediction of the stretching frequency of the V=O bond with hybrid functionals such as B3LYP and B3P86 is slightly superior than that with the GGA PBE functional and that B3LYP performs better than B3P86, even if the deviation of about 10% is in agreement with the data in the literature.[29c] In this work, the stretching frequency of V=O bond ($\nu_{V=O}$) for solid complexes of salicylaldiminate and aminophenolate ligands was calculated with the B3LYP functional and the triple zeta basis set 6-311G. The values predicted for the series $[VO(MeSal)_2]$, $[VO(i\text{Pr-MeSal})_2]$ and $[VO(t\text{Bu-MeSal})_2]$ are 1049.6, 1041.0 and 1037.5 cm^{-1} (experimental values: 980, 976 and 968 cm^{-1})[13] and for $[VO(NMe_2phen)_2]$, $[VO(Pip\text{-}4Mephen)_2]$ and $[VO(NMe_2\text{-}t\text{Buphen})_2]$ 1028.9, 1024.7 and 1006.8 cm^{-1}, respectively. For $V^{IV}O^{2+}$ species formed by salicylaldiminate ligands the values are overestimated with a mean deviation of 7.0%. The predicted trend reflects the length of the V=O bond that increases with increasing the trigonal bipyramidal distortion {experimental V=O distance of 1.590, 1.599 and 1.601 Å for $[VO(MeSal)_2]$, $[VO(i\text{Pr-MeSal})_2]$ and $[VO(t\text{Bu-MeSal})_2]$}.

The calculated variation of $\nu_{V=O}$ with τ for salicylaldiminate and aminophenolate species is reported in Figure 9 (it must be highlighted that experimental values for the V=O stretching for the latter compounds are not reported in the literature); the decrease of $\nu_{V=O}$ with the distortion is easily observed and must be taken into account in the analysis of a $V^{IV}O^{2+}$ structure for which X-ray crystallographic data are not available.

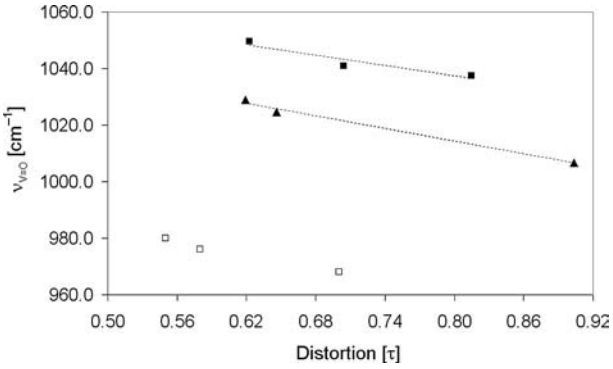

Figure 9. Variation of the $\nu_{V=O}$ value as a function of τ for $V^{IV}O^{2+}$ complexes formed by salicylaldiminate (squares) and aminophenolate ligands (triangles). The calculated and experimental values are shown as filled and empty symbols, respectively.

Variation of the ^{14}N Superhyperfine Coupling Constant (A^N)

ESEEM is a variant of EPR spectroscopy, which can provide information on the superhyperfine coupling between the unpaired electron on vanadium and the nuclei in the ligand sphere, indicated by the constant A^L.[38] The superhyperfine coupling constants reported for ^{14}N are in

Table 6. ^{14}N superhyperfine coupling constants, ^{51}V nuclear quadrupolar coupling constants and asymmetry parameter obtained from DFT calculations of the $V^{IV}O^{2+}$ complexes formed by aminophenolate ligands.[a]

Complex	$\lvert A_{iso}^N\rvert^{calcd.}$	$\lvert A_{iso}^N\rvert^{exp.}$	$\lvert A_x^N\rvert^{calcd.}$	$\lvert A_y^N\rvert^{calcd.}$	$\lvert A_z^N\rvert^{calcd.}$	$\lvert A_x^N\rvert^{exp.}$	$\lvert A_y^N\rvert^{exp.}$	$\lvert A_z^N\rvert^{exp.}$	$\lvert C_Q\rvert$	η
$[VO(NMe_2phen)_2]$	4.45	4.75	4.65	4.50	4.19	4.80	4.70	4.70	8.26	0.710
$[VO(Pip\text{-}4Mephen)_2]$	4.43	4.70	4.68	4.47	4.15	4.70	4.60	4.85	8.17	0.690
$[VO(NMe_2\text{-}t Buphen)_2]$	4.22	4.65	4.47	4.26	3.92	4.60	4.50	4.85	7.34	0.461

[a] Values of the ^{14}N superhyperfine coupling constants and ^{51}V nuclear quadrupolar coupling constants given in MHz.

the range 1–8 MHz and vary with the nature, position and orientation of the ligand.[39]

To date, few computational studies have been published in which ligand superhyperfine coupling constants for transition metal complexes were calculated,[40,41] and, to the best of our knowledge, only one study concerns a $V^{IV}O^{2+}$ ion.[41] We recently obtained encouraging results using the complex $[VO(hybeb)_2]^{2-}$ [H_4hybeb = 1,2-bis(2-hydroxybenzamido)benzene] as a benchmark for which the experimental values of A^N are known; the best results have been obtained with the half-and-half functional BHandH and the basis set 6-311G(d,p) or 6-311+G(d,p).[29b]

The superhyperfine coupling constants with the ^{14}N nucleus in the $V^{IV}O^{2+}$ species formed with amoniphenolate ligands, for which the experimental data are reported in the literature,[15] were calculated. The calculated and experimental A^N values are listed in Table 6. As noted in the literature,[39a] the components of $\boldsymbol{A}^N$ tensor are negative, but for convenience of interpretation only their absolute values are reported.

The values of $|A_{iso}^N|$ are in good agreement with those observed experimentally and are as expected for an sp^3-amino nitrogen atom (ca. 5 MHz).[39a,39b] In Figure 10, the variation of $|A_{iso}^N|$ with τ is shown; a slight decrease can be observed, even if the differences between $|A_{iso}^N|$ are small and almost within the experimental error. Fukui et al. have reported that the values of $|A_{iso}^N|$ of $V^{IV}O^{2+}$complexes are related to the sp^n character of the nitrogen lone-pair and should increase with the *s*-character of the bond.[39a] As a matter of fact, the tetrahedral character of the amine nitrogen atom in $[VO(NMe_2phen)_2]$ (mean value of C–N–C 110.3°), $[VO(Pip\text{-}4Mephen)_2]$ (111.3°) and $[VO(NMe_2\text{-}t Buphen)_2]$ (110.0°) and, consequently, the *s*-character of the V–N bond varies very slightly with trigonal bipyramidal distortion. Van Koten and coworkers also proposed that the basicity of the nitrogen atoms and the presence of electron donating or withdrawing groups on the ligands may determine the differences observed and disturb this correlation.[15]

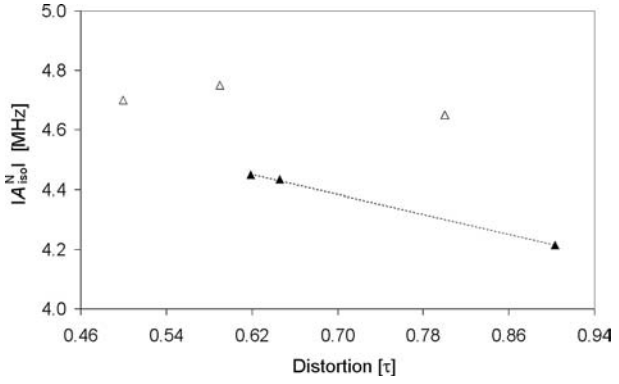

Figure 10. Variation of the $|A_{iso}^N|$ value as a function of τ for $V^{IV}O^{2+}$ complexes formed by aminophenolate ligands. The calculated and experimental values are shown as filled and empty symbols, respectively.

Variation of ^{51}V Nuclear Quadrupolar Coupling Constants (C_Q) and the Asymmetry Parameter (η)

The ^{51}V nuclear quadrupole coupling constant (C_Q) is the coupling between the nuclear quadrupole moment of the vanadium nucleus and the electric field gradient (EFG) at the nucleus due to nonspherical charge distribution. Values of C_Q for vanadium are sensitive to axial ligation,[42] the coordination geometry and structural distortions of a $V^{IV}O^{2+}$ species.[43] Another parameter related to C_Q is the asymmetry parameter $\eta = (V_x - V_y)/V_z$, where V_x, V_y and V_z are the components of the EFG. To the best of our knowledge, this is the first attempt to calculate C_Q for $V^{IV}O^{2+}$ complexes. We used the same level of theory that yielded good results in the prediction of C_Q^N for $[VO(hybeb)]^{2-}$, namely, the functional B3PW91 and basis set 6-311g(d,p).[29b]

The values of C_Q and η for the complexes studied are listed in Table 6. The variation of C_Q and η as a function of the trigonal bipyramidal distortion is represented in Figures S3 and S4 (Supporting Information), where it can be seen that a significant decrease of both the values is expected. This is in agreement with the observations of Britt and coworkers who demonstrated that the experimental value of C_Q for a series of pentacoordinate $V^{IV}O^{2+}$ complexes decreases with the increasing distortion towards the trigonal bipyramid.[43] Since C_Q is dependent on the EFG at the vanadium nucleus and the oxido bond establishes the majority of the gradient along the V=O bond axis, they showed that the trigonal bipyramidal distortion allows for an increase in electron density donation opposite to the oxido bond and diminishes the EFG established by such a bond;[43] consequently, the magnitude of C_Q significantly decreases. A linear relationship between the experimental value of C_Q and τ was obtained;[43] our results in Figure S3 confirm these findings. A similar trend of the values of η with the trigonal bipyramidal distortion is predicted by DFT methods (Figure S4). It will be interesting to know if the experimental measurement of η will confirm these suppositions in the future.

Conclusions

Depending on the steric hindrance of the ligand and degree of solvation of the complex, a pentacoordinate species formed by $V^{IV}O^{2+}$ can be significantly distorted towards the trigonal bipyramid. This distortion can influence the chemical behaviour and the enzymatic and/or biological activity. In this work we studied three different classes of $V^{IV}O^{2+}$ complexes (formed by α-hydroxycarboxyate, salicylaldiminate and aminophenolate ligands) with DFT methods and analysed the variation of the structural, electronic and spectroscopic parameters as a function of the structural index of trigonality (τ). Beyond the theoretical aspects of the simulations, our goal is to provide an operative tool to predict the distortion of a $V^{IV}O^{2+}$ species in the absence of X-ray diffractometric analysis.

The results indicate that the distortion is influenced not only by the steric hindrance of the substituents on the α-carbon atom but also by the hydrophobicity of the complexes. Moreover, on the basis of the DFT calculations, with increasing the value of τ we expect: i) an increase of $|A_x - A_y|$, which measures the anisotropy of an EPR spectrum in the x,y region, ii) a decrease of the ^{51}V isotropic hyperfine coupling constant, $|A_{iso}|$, iii) a decrease of the ^{51}V anisotropic coupling constant along the z axis, $|A_z|$, iv) an increase of the $|g_x - g_y|$ parameter, v) a decrease of $\Delta\lambda = \lambda_2 - \lambda_3$, where λ_2 and λ_3 are the second and third absorption in the four band electronic spectrum, vi) an increase of λ_1, the lowest energy electronic transition, vii) a decrease of $\nu_{V=O}$, the stretching vibration of the V=O bond, viii) a slight decrease of $|A_{iso}^N|$, the superhyperfine coupling constant with the ^{14}N nucleus measurable in an ESEEM spectrum, ix) a decrease of the ^{51}V C_Q and x) a decrease of the asymmetry parameter $\eta = (V_x - V_y)/V_z$.

As a final comment, however, it must be noted that the detection of the variation predicted is dependent on being able to determine the spectroscopic parameters with a high degree of accuracy. In some cases (particularly, correlations involving g and $|A_{iso}^N|$ values), the change expected with trigonal bipyramidal distortion is smaller than the uncertainty with which they can be determined.

Computational Section

DFT Calculations: All the calculations presented in this paper were performed with Gaussian 03 (revision C.02)[20] or ORCA (version 2.8–20) programs.[32] The hybrid exchange-correlation functional B3LYP[22,23] and B3PW91,[22,44] and the half-and-half BHandHLYP and BHandH, as incorporated in Gaussian 03, were used.

The structures of $V^{IV}O^{2+}$ complexes were optimized in the gas phase and in solution employing the hybrid exchange-correlation functional B3LYP. The solvent (H_2O for α-hydroxycarboxylate and salicylaldiminate complexes, and Et_2O for aminophenolate complexes) was simulated within the framework of the polarizable continuum model.[21] The geometries were preoptimized at the B3LYP/sto-3G level and further optimized at the B3LYP/6-311G level of theory. For all the structures, minima were verified through frequency calculations.

The optimized structures were used to calculate the spectroscopic parameters at the following level of theory: ^{51}V hyperfine (A_{iso}, A_x, A_y and A_z) coupling constants at BHandHLYP/6-311G(d,p), g values at B3LYP/TZVP with ORCA, the stretching frequency of the V=O bond ($\nu_{V=O}$) at B3LYP/6/311g, ^{14}N superhyperfine coupling constants ($|A_{iso}^N|$, $|A_x^N|$, $|A_y^N|$ and $|A_z^N|$) at BHandH/6-311G(d,p), ^{51}V C_Q at B3PW91/6-311G(d,p). TD-DFT calculations were performed at the B3LYP/6-31G level and used to predict the excited states of the $V^{IV}O^{2+}$ species and calculate the electronic absorption spectra.

The variation of the total energy of $[VO(glycH_{-1})_2]^{2-}$ and $[VO(2\text{-}i\text{PrhbH}_{-1})_2]^{2-}$ as a function of τ was calculated by freezing the axial and equatorial angles O–V–O at values symmetrical with respect to that of equilibrium and calculating the energies of the species obtained both in the gas phase and in water; for example, if the angles at equilibrium for $[VO(glycH_{-1})_2]^{2-}$ are 154.60 and 131.83° (τ = 0.38), respectively, the adjacent points were calculated by freezing the angles at 154.02 and 132.40° (τ = 0.36) and 155.22 and 131.22° (τ = 0.40), respectively.

The analysis of MO composition in terms of atomic orbitals or groups of atoms was performed using the AOMix program.[45]

Theory Background: $V^{IV}O^{2+}$ ion has a d^1 electronic configuration with one unpaired electron. The hyperfine coupling constants in an EPR spectrum arise from the interaction between the spin angular momentum of the electron (S = 1/2) with the spin angular momentum of ^{51}V nucleus (I = 7/2, 99.8% natural abundance). In the first-order approximation, the $\boldsymbol{A}$ tensor has one isotropic contribution deriving from the Fermi contact (A_{iso}) and another from the dipolar hyperfine interaction ($\boldsymbol{T}$ tensor): $\boldsymbol{A} = A_{iso}1 + \boldsymbol{T}$.[46] The values of the ^{51}V anisotropic hyperfine coupling constant along the x, y and z axes can be calculated by the equations: $A_x^{calcd.} = A_{iso} + T_x$; $A_y^{calcd.} = A_{iso} + T_y$; $A_z^{calcd.} = A_{iso} + T_z$, with T_x, T_y and T_z being the components of $\boldsymbol{T}$. The tensor $\boldsymbol{T}$ is traceless ($T_x + T_y + T_z = 0$), so that $A_{iso} = 1/3\ (A_x + A_y + A_z)$. The A_z value (as well as A_x and A_y) is negative but the absolute value is usually reported in the literature; therefore, the percentage deviation from the experimental value is calculated as $100 \times (|A_z|^{calcd.} - |A_z|^{exp.})/|A_z|^{exp.}$.

The ^{51}V C_Q was evaluated from the EFG tensor, $\boldsymbol{V}$, a traceless second-rank tensor.[47] C_Q is defined by eQV_z/h, where e is the charge of an electron, Q is the ^{51}V nuclear quadrupole moment, V_z is the largest component of the EFG and h is Planck's constant. For the ^{51}V nucleus, Q is -4.8×10^{-24} m^2, the value of -5.2×10^{-24} m^2 commonly reported has recently been revised.[48] The asymmetry parameter is given by the expression $\eta = (V_x - V_y)/V_z$, with $|V_z| \geq |V_y| \geq |V_z|$.

Supporting Information (see footnote on the first page of this article): tables with atomic coordinates for all optimised structures (Tables S1–S22), figures with representative MOs of $[VO(2\text{-}i\text{PrhbH}_{-1})_2]^{2-}$ (Figure S1), with the variation of the dipolar tensor components as a function of τ (Figure S2), with the variation of $|C_Q|$ as a function of τ (Figure S3), with the variation of η as a function of τ (Figure S4) and a scheme with the relative energy levels of the MOs of $[VO(glycH_{-1})_2]^{2-}$, $[VO(MeSal)_2]$ and $[VO(NMe_2phen)_2]$ (Scheme S1).

[1] a) D. C. Crans, J. J. Smee, E. Gaidamauskas, L. Yang, *Chem. Rev.* **2004**, *104*, 849–902; b) D. Rehder, *Bioinorganic Vanadium Chemistry*, Wiley, Chichester, **2008**.
[2] J. Costa Pessoa, I. Tomaz, *Curr. Med. Chem.* **2010**, *17*, 3701–3738, and references cited therein.
[3] a) Y. Shechter, S. J. D. Karlish, *Nature* **1980**, *284*, 556–558; b) K. H. Thompson, J. H. McNeill, C. Orvig, *Chem. Rev.* **1999**,

99, 2561–2571, and references cited therein; c) K. H. Thompson, C. Orvig, *Coord. Chem. Rev.* **2001**, *219–221*, 1033–1053, and references cited therein; d) Y. Shechter, I. Goldwaser, M. Mironchik, M. Fridkin, D. Gefel, *Coord. Chem. Rev.* **2003**, *237*, 3–11; e) H. Sakurai, Y. Yoshikawa, H. Yasui, *Chem. Soc. Rev.* **2008**, *37*, 2383–2392.

[4] D. C. Crans, A. S. Tracey, in: *Vanadium Compounds: Chemistry, Biochemistry and Therapeutic Applications* (Eds.: A. S. Tracey, D. C. Crans), ACS symposium series 711, Washington DC, **1998**, p. 2–29.

[5] a) K. Kustin, W. E. Robinson, in: *Metal Ions in Biological Systems* (Eds.: A. Sigel, H. Sigel), Marcel Dekker, New York, **1995**, vol. 31, p. 511–542; b) F. H. Nielsen, in *Vanadium Compounds: Chemistry, Biochemistry and Therapeutic Applications* (Eds.: A. S. Tracey, D. C. Crans), ACS symposium series 711, Washington DC, **1998**, p. 297–315; c) T. Kiss, T. Jakusch, D. Hollender, A. Dörnyei, E. A. Enyedy, J. Costa Pessoa, H. Sakurai, A. Sanz-Medel, *Coord. Chem. Rev.* **2008**, *252*, 1153–1162, and references cited therein.

[6] G. Santoni, D. Rehder, *J. Inorg. Biochem.* **2004**, *98*, 758–764.

[7] F. Neese, *Coord. Chem. Rev.* **2009**, *253*, 526–563, and references cited therein.

[8] P. Comba, M. Kerscher, *Coord. Chem. Rev.* **2009**, *253*, 564–574.

[9] C. E. Schäffer, C. Anthon, J. Bendix, *Coord. Chem. Rev.* **2009**, *253*, 575–593.

[10] R. J. Deeth, A. Anastasi, C. Diedrich, K. Randell, *Coord. Chem. Rev.* **2009**, *253*, 795–816.

[11] C. J. Ballhausen, H. B. Gray, *Inorg. Chem.* **1962**, *1*, 111–122.

[12] A. W. Addison, T. N. Rao, J. Reedijk, J. van Rijn, G. C. Verschoor, *J. Chem. Soc., Dalton Trans.* **1984**, 1349–1356.

[13] C. R. Cornman, K. M. Geisre-Bush, S. R. Rowley, P. D. Boyle, *Inorg. Chem.* **1997**, *36*, 6401–6408.

[14] E. Garribba, G. Micera, A. Panzanelli, D. Sanna, *Inorg. Chem.* **2003**, *42*, 3981–3987.

[15] H. Hagen, S. Reinoso, E. J. Reijerse, E. E. van Faassen, M. Lutz, A. L. Spek, G. van Koten, *Z. Anorg. Allg. Chem.* **2004**, *630*, 2097–2105.

[16] G. Micera, D. Sanna, A. Dessì, T. Kiss, P. Buglyó, *Gazz. Chim. Ital.* **1993**, *123*, 573–577.

[17] H. Hagen, A. Barbon, E. E. van Faassen, B. T. G. Lutz, J. Boersma, A. L. Spek, G. van Koten, *Inorg. Chem.* **1999**, *38*, 4079–4086.

[18] As usual, the negative index for protons indicates the dissociation of groups that do not deprotonate in the absence of $V^{IV}O^{2+}$ coordination. The five α-hydroxycarboxylic acids, the three salicylaldimine derivatives and the three aminophenols can be indicated with LH, where the proton belongs to the carboxylic group in the first case and to the phenolic –OH in the other two. In the presence of the metal ion, for α-hydroxycarboxylic acids both the –COOH and alcoholic –OH group undergo deprotonation, so that they coordinate $V^{IV}O^{2+}$ ion in the LH_{-1}^{2-} form, whereas for salicylaldimine and aminophenol derivatives only the phenolic –OH loses its proton and they bind vanadium in the L^- form.

[19] N. D. Chasteen, R. L. Belford, I. C. Paul, *Inorg. Chem.* **1969**, *8*, 408.

[20] M. J. Frisch, G. W. Trucks, H. B. Schlegel, G. E. Scuseria, M. A. Robb, J. R. Cheeseman, J. A. Montgomery Jr., T. Vreven, K. N. Kudin, J. C. Burant, J. M. Millam, S. S. Iyengar, J. Tomasi, V. Barone, B. Mennucci, M. Cossi, G. Scalmani, N. Rega, G. A. Petersson, H. Nakatsuji, M. Hada, M. Ehara, K. Toyota, R. Fukuda, J. Hasegawa, M. Ishida, T. Nakajima, Y. Honda, O. Kitao, H. Nakai, M. Klene, X. Li, J. E. Knox, H. P. Hratchian, J. B. Cross, C. Adamo, J. Jaramillo, R. Gomperts, R. E. Stratmann, O. Yazyev, A. J. Austin, R. Cammi, C. Pomelli, J. W. Ochterski, P. Y. Ayala, K. Morokuma, G. A. Voth, P. Salvador, J. J. Dannenberg, V. G. Zakrzewski, S. Dapprich, A. D. Daniels, M. C. Strain, O. Farkas, D. K. Malick, A. D. Rabuck, K. Raghavachari, J. B. Foresman, J. V. Ortiz, Q. Cui, A. G. Baboul, S. Clifford, J. Cioslowski, B. B. Stefanov, G. Liu, A. Liashenko, P. Piskorz, I. Komaromi, R. L. Martin, D. J. Fox, T. Keith, M. A. Al-Laham, C. Y. Peng, A. Nanayakkara, M. Challacombe, P. M. W. Gill, B. Johnson, W. Chen, M. W. Wong, C. Gonzalez, J. A. Pople, *Gaussian 03*, rev. C.02, Gaussian, Inc., Wallingford CT, **2004**.

[21] a) S. Miertus, E. Scrocco, J. Tomasi, *Chem. Phys.* **1981**, *55*, 117–129; b) S. Miertus, J. Tomasi, *Chem. Phys.* **1982**, *65*, 239–245; c) M. Cossi, V. Barone, R. Cammi, J. Tomasi, *Chem. Phys. Lett.* **1996**, *255*, 327–335.

[22] A. D. Becke, *J. Chem. Phys.* **1993**, *98*, 5648–5652.

[23] C. Lee, W. Yang, R. G. Parr, *Phys. Rev. B* **1988**, *37*, 785–789.

[24] a) K. G. Spears, *J. Phys. Chem. A* **1997**, *101*, 6273–6279; b) C. P. Aznar, Y. Deligiannakis, E. J. Tolis, T. Kabanos, M. Brynda, R. D. Britt, *J. Phys. Chem. A* **2004**, *108*, 4310–4321; c) I. Correia, J. Costa Pessoa, M. T. Duarte, R. T. Henriques, M. F. M. Piedade, L. F. Veiros, T. Jakusch, A. Dornyei, T. Kiss, M. M. C. A. Castro, C. F. G. C. Geraldes, F. Avecilla, *Chem. Eur. J.* **2004**, *10*, 2301–2317; d) K. Zborowski, R. Grybos, L. M. Proniewicz, *Inorg. Chem. Commun.* **2005**, *8*, 76–78; e) K. J. Ooms, S. E. Bolte, J. J. Smee, B. Baruah, D. C. Crans, T. Polenova, *Inorg. Chem.* **2007**, *46*, 9285–9293; f) L. L. G. Justino, M. L. Ramos, F. Nogueira, A. J. F. N. Sobral, C. F. G. C. Geraldes, M. Kaupp, H. D. Burrows, C. Fiolhais, V. M. S. Gil, *Inorg. Chem.* **2008**, *47*, 7317–7326.

[25] G. Micera, E. Garribba, *Int. J. Quantum Chem.* **2011**; DOI: 10.1002/qua.23237.

[26] G. Micera, E. Garribba, *Dalton Trans.* **2009**, 1914–1918.

[27] E. Lodyga-Chruscinska, D. Sanna, E. Garribba, G. Micera, *Dalton Trans.* **2008**, 4903–4916.

[28] M. Bühl, C. Reimann, D. A. Pantazis, T. Bredow, F. Neese, *J. Chem. Theory Comput.* **2008**, *4*, 1449–1459.

[29] a) S. Gorelsky, G. Micera, E. Garribba, *Chem. Eur. J.* **2010**, *16*, 8167–8180; b) G. Micera, E. Garribba, *Eur. J. Inorg. Chem.* **2010**, 4697–4710; c) E. Lodyga-Chruscinska, G. Micera, E. Garribba, *Inorg. Chem.* **2011**, *50*, 883–899.

[30] a) *Calculation of NMR and EPR Parameters. Theory and Applications* (Eds: M. Kaupp, M. Bühl, V. G. Malkin), Wiley-VCH, Weinheim, Germany, **2004**; b) C. Remenyi, R. Reviakine, A. V. Arbuznikov, J. Vaara, M. Kaupp, *J. Phys. Chem. A* **2004**, *108*, 5026–5033, and references cited therein.

[31] a) M. L. Munzarová, M. Kaupp, *J. Phys. Chem. B* **2001**, *105*, 12644–12652, and references cited therein; b) A. C. Saladino, S. C. Larsen, *J. Phys. Chem. A* **2003**, *107*, 1872–1878; c) F. Neese, *J. Chem. Phys.* **2003**, *118*, 3939–3948; d) C. P. Aznar, Y. Deligiannakis, E. J. Tolis, T. Kabanos, M. Brynda, R. D. Britt, *J. Phys. Chem. A* **2004**, *108*, 4310–4321; e) A. C. Saladino, S. C. Larsen, *Catal. Today* **2005**, *105*, 122–133, and references cited therein.

[32] F. Neese, *ORCA* – an ab initio, DFT and semiempirical program package, 2.8–20 ed., University of Bonn, Germany, **2010**.

[33] F. Neese, *Mol. Phys.* **2007**, *105*, 2507–2514.

[34] a) E. Runge, E. K. U. Gross, *Phys. Rev. Lett.* **1984**, *52*, 997–1000; b) M. E. Casida, in: *Recent Advances in Density Functional Methods* (Ed.: D. P. Chong), World Scientific, Singapore, **1995**, vol. 1, p. 155–192.

[35] A. Rosa, G. Ricciardi, O. Gritsenko, E. J. Berends, *Struct. Bonding (Berlin)* **2004**, *112*, 49–115.

[36] W. Koch, M. C. Holthausen, *A Chemist's Guide to Density Functional Theory*, 2nd Ed., Wiley-VCH, Weinheim, **2001**.

[37] J. Neugebauer, B. A. Hess, *J. Chem. Phys.* **2003**, *118*, 7215–7225.

[38] a) A. Schweiger, *Angew. Chem.* **1991**, *103*, 223; *Angew. Chem. Int. Ed. Engl.* **1991**, *30*, 265–292; b) S. A. Dikanov, Y. D. Tsvetkov, *Electron Spin Echo Envelope Modulation (ESEEM) Spectroscopy*, CRC Press, Boca Raton, **1992**; c) Y. Deligiannakis, M. Louloudi, N. Hadjiliadis, *Coord. Chem. Rev.* **2000**, *204*, 1–112; d) T. S. Smith II, R. LoBrutto, V. L. Pecoraro, *Coord. Chem. Rev.* **2002**, *228*, 1–18.

[39] a) K. Fukui, H. Ohya-Nishiguchi, H. Kamada, *Inorg. Chem.* **1997**, *36*, 5518–5529, and references cited therein; b) K. Fukui, H. Ohya-Nishiguchi, H. Kamada, M. Iwaizumi, Y. Xu, *Bull. Chem. Soc. Jpn.* **1998**, *71*, 2787–2796, and references cited therein; c) R. LoBrutto, B. J. Hamstra, G. J. Colpas, V. L. Pecoraro, W. D. Frasch, *J. Am. Chem. Soc.* **1998**, *120*, 4410–4416; d) K. Fukui, H. Fujii, H. Ohya-Nishiguchi, H. Kamada, *Chem. Lett.* **2000**, 198–199; e) K. Fukui, T. Ueki, H. Ohya, H. Michibata, *J. Am. Chem. Soc.* **2003**, *125*, 6352–6353.
[40] a) R. G. Hayes, *Inorg. Chem.* **2000**, *39*, 156–158; b) F. Neese, *J. Phys. Chem. A* **2001**, *105*, 4290–4299; c) W. M. Ames, S. C. Larsen, *Phys. Chem. Chem. Phys.* **2009**, *11*, 8266–8274.
[41] A. C. Saladino, S. C. Larsen, *J. Phys. Chem. A* **2003**, *107*, 4735–4740.
[42] C. V. Grant, J. A. Ball, B. J. Hamstra, V. L. Pecoraro, R. D. Britt, *J. Phys. Chem. B* **1998**, *102*, 8145–8150.
[43] K. M. Geiser-Bush, C. R. Cornman, R. D. Britt, *Inorg. Chem.* **1999**, *38*, 6285–6288.
[44] a) J. P. Perdew, in: *Electronic Structure of Solids* (Eds.: P. Ziesche, H. Eischrig), Akademie Verlag, Berlin, **1991**; b) J. P. Perdew, Y. Wang, *Phys. Rev. B* **1992**, *45*, 13244–13249.
[45] a) S. I. Gorelsky, AOMix program, rev. 6.52 (http://www.sgchem.net, University of Ottawa, Ottawa, **2011**); b) S. I. Gorelsky, A. B. P. Lever, *J. Organomet. Chem.* **2001**, *635*, 187–196.
[46] a) R. S. Drago, *Physical Methods in Chemistry*, Saunders, Philadelphia, **1977**; b) J. E. Wertz, J. R. Bolton, *Electron Spin Resonance: Elementary Theory and Practical Applications*, Chapman and Hall, New York, **1986**.
[47] E. A. C. Lucken, *Nuclear Quadrupole Coupling Constants*, Academic Press, New York, **1969**.
[48] D. Rehder, T. Polenova, M. Bühl, *Annu. Rep. NMR Spectrosc.* **2007**, *62*, 49–114.

Received: April 19, 2011
Published Online: August 5, 2011

